Local character of the highest antiferromagnetic temperature of Ce systems in Sc-rich $CeTi_{1-x}Sc_xGe$

J. G. Sereni, P. Pedrazzini, M. Gómez Berisso, A. Chacoma, and S. Encina
Low Temperature Division, CAB-CNEA and Instituto Balseiro, 8400 San Carlos de Bariloche, Argentina

T. Gruner, N. Caroca-Canales, and C. Geibel
Max-Planck Institute for Chemical Physics of Solids, D-01187 Dresden, Germany
(Received 13 February 2015; revised manuscript received 21 April 2015; published 7 May 2015)

The highest antiferromagnetic (AFM) temperature in Ce based compounds has been reported for CeScGe with $T_N = 47$ K, but its local or itinerant nature has not been deeply investigated yet. In order to shed more light into this unusually high ordering temperature we have investigated structural, magnetic, transport, and thermal properties of $CeTi_{1-x}Sc_xGe$ alloys within the range of stability of the CeScSi-type structure: $0.25 \leqslant x \leqslant 1$. Along this concentration range, this strongly anisotropic system presents a complex magnetic phase diagram with a continuous modification of its magnetic behavior, from ferromagnetism for $0.25 \leqslant x \leqslant 0.50$ (with 7 K $\leqslant T_C \leqslant$ 16 K) to AFM for $0.60 \leqslant x \leqslant 1$ (with 19 K $\leqslant T_N \leqslant$ 47 K). The onset of the AFM phase is associated to a metamagnetic transition with a critical field increasing from $H_{cr} = 0$ at $x \approx 0.55$ to $\approx$6 T at $x = 1$, coincident with an increasing contribution of the first excited crystal electric field doublet. At a critical point $x_{cr} \approx 0.65$ a second transition appears at $T_L \leqslant T_N$. In contrast to observations in itinerant systems like $CeRh_2Si_2$ or $CeRh_3B_2$, no evidences for significant hybridization of the $4f$ electrons at large Sc contents were found. Therefore, the exceptionally large T_N of CeScGe can be attributed to an increasing Ruderman-Kittel-Kasuya-Yosida interaction between Ce double layers as Sc content grows.

DOI: 10.1103/PhysRevB.91.174408 PACS number(s): 75.20.Hr, 71.27.+a, 75.30.Kz, 75.10.−b

I. INTRODUCTION

Long range magnetic order of cerium ions can be found along four decades of temperature, from 1.6 mK in CMN [1] up to 115 K in $CeRh_3B_2$ [2], though most known transitions occur between a few degrees and $T_{ord} \approx 12$ K. Different temperature ranges of magnetic order are characterized by different magnetic behaviors. While magnetic interactions between localized Ce-$4f$ moments are typically observed for $T_{ord} < 12$ K [3], in the cases where T_{ord} exceeds that temperature, two types of behaviors can be distinguished. The one with localized Ce-$4f$ moments is related to the rare cases of Ce binary compounds formed in cubic-bcc structure. This is the crystal structure with the highest symmetry that allows one to have the Γ_8 quartet as the ground state. However, its fourfold degeneracy is reduced by undergoing different types of transitions mostly connected with structural modifications. Those compounds are CeZn ($T_N = 30$ K), CeTl ($T_N = 25.5$ K), CeMg ($T_C = 20$ K), CeCd ($T_C = 16.5$ K), and CeAg ($T_N = 15.6$ K) [4].

The ternary Ce-based compounds belonging to the other group show evidences of itinerant character [5]. Among them, the outstanding case is the above mentioned $CeRh_3B_2$ that shows the highest ordering temperature with $T_{ord} = 115$ K [2]. The following highest ordering temperature has been reported for CeScGe with $T_{ord} = 47$ K [6], but the local or itinerant nature of its magnetic state is under discussion. Within this group, one of the most studied compounds is $CeRh_2Si_2$, which shows a $T_{ord} = 36$ K [7,8]. Also in this case evidences for local and itinerant magnetic character were equally claimed by different authors [9–11].

Such ambiguity, that appears frequently in Ce compounds, was identified as the local-itinerant dilemma of Ce-$4f$ electrons [12]. The eventual itinerant character of the $4f$ orbitals was compared to the U-$5f$ behavior [5], whose compounds frequently show high T_{ord} values with clear itinerant characteristics arising from the extended character of the $5f$ orbitals. In Ce-$4f$ systems, however, itineracy is related to some degree of hybridization with the conduction band and the consequent weakening of the $4f$ effective magnetic moment, μ_{eff}. In terms of Doniach model [13], the question arises whether there is an optimal combination of weak $4f$-band hybridization that enhances the intersite RKKY interaction by increasing the in-site $4f$-band exchange without reducing μ_{eff} significantly.

In the case of CeScGe, it was formerly reported as a ferromagnet (FM) [6] that usually implies local $4f$ character. However, band-structure calculations [14], based on itinerant character, suggested that FM and antiferromagnetic (AFM) states compete in energy. A subsequent study on CeScSi and CeScGe [15] recognized both compounds as AFM. Thus CeScGe presents the best characteristics for the proposed investigation.

A further aspect that has to be taken into account for a proper knowledge of the ordered phase at those temperatures is the role of the excited crystal-electric-field (CEF) levels. This contribution can be properly evaluated by tracing T_{ord} from relatively low values, where only a doublet with local-$4f$ character contributes to the magnetic ground state, to high values where involvement of excited CEF levels becomes very likely. These conditions are fulfilled by $CeTi_{1-x}Sc_xGe$ alloys, that cover an extended range of transition temperatures from $T_{ord} \approx 7$ K in $CeTi_{0.75}Sc_{0.25}Ge$ to $T_{ord} \approx 47$ K at the stoichiometric limit CeScGe [6]. The lowest T_{ord} value is determined by the limit of stability of the CeScSi-type structure (at $x = 0.25$) on the Ti rich side. Below $x \approx 0.15$ this alloy stabilizes in the CeFeSi-type structure.

II. EXPERIMENTAL DETAILS AND RESULTS

Polycrystalline samples of $CeTi_{1-x}Sc_xGe$ with $0.25 \leqslant x \leqslant 1$ were synthesized by arc melting under Ar atmosphere the nominal amounts of the constituents with purity above 99.99%. The samples were turned over and remelted several times to ensure homogeneity. Then, the samples were placed in a tungsten boat wrapped with zirconium foil and annealed at 1200 °C for one week. The quality of the samples was verified by means of x-ray powder-diffraction measurements using Cu-$K\alpha_1$ radiation ($\lambda = 1.54056$ Å) in a Stoe-Stadip-MP diffractometer. The pattern was indexed on the basis of the tetragonal CeScSi-type structure.

Specific heat was measured between 0.5 and 50 K using a standard heat pulse technique in a semiadiabatic He^3 calorimeter. The magnetic contribution C_m is obtained by subtracting the phonon contribution extracted from $LaTi_{0.5}Sc_{0.5}Ge$. Magnetization measurements were carried out using a Quantum Design MPMS magnetometer operating between 2 and 300 K, and as a function of field up to 50 kOe. Electrical resistivity was measured between 2 K and room temperature using a standard four probe technique with an LR700 resistance bridge.

A. Structural properties

The $CeTi_{1-x}Sc_xGe$ system forms in two related crystal structures: CeFeSi-type for low Sc content (up to $x = 0.15$) and CeScSi-type beyond $x = 0.23$ [16]. In the latter, each second Ce-double layer is shifted by (1/2, 1/2) with a rearrangement of Sc and Si atoms, becoming a body centered tetragonal instead of primitive tetragonal of CeFeSi, see Fig. 1, with the consequent doubling of the c lattice parameter.

Sc concentration x dependencies of the unit cell volume $V(x)$ and the c/a ratio of tetragonal lattice parameters are shown in Fig. 2. Both parameters show a linear dependence within the expected experimental dispersion. The increase of $V(x)$ can be explained by the larger atomic volume of Sc with respect to Ti, whereas the reduction of the c/a ratio is due to the increase of the a parameter because c remains practically unchanged. This indicates that an expansion in the basal plane of the tetragonal structure occurs, whereas the interlayer distances in the c axis direction are only slightly affected.

B. Magnetic susceptibility

In Fig. 3, the inverse of the high temperature magnetic susceptibility ($1/\chi$) is presented after subtracting a Pauli type paramagnetic contribution χ_P. This temperature independent contribution, already reported for CeScGe [17], is observed to decrease from $\chi_P = 0.9 \times 10^{-3}$ at $x = 0.4$ to 0.47×10^{-3} emu/Oe mol at $x = 1$, as shown in the inset of Fig. 3. The $1/\chi$ dependence on concentration (evaluated for $T > 50$ K) indicates a decrease of Ce effective magnetic moment from $\mu_{\text{eff}}(x) \approx 2.25\mu_B$ at $x = 0.4$ to $\approx 2\mu_B$ at $x = 0.7$. Beyond that concentration $\mu_{\text{eff}}(x)$ remains practically unchanged. Notably, the paramagnetic temperature $\theta_P(x)$ is positive along the full concentration range and even increases from $\theta_P \approx 8$ K at $x = 0.4$, up to 19 K at $x = 0.8$. At that concentration it slightly decreases down to 17 K at $x = 1$ as shown in the inset of Fig. 3.

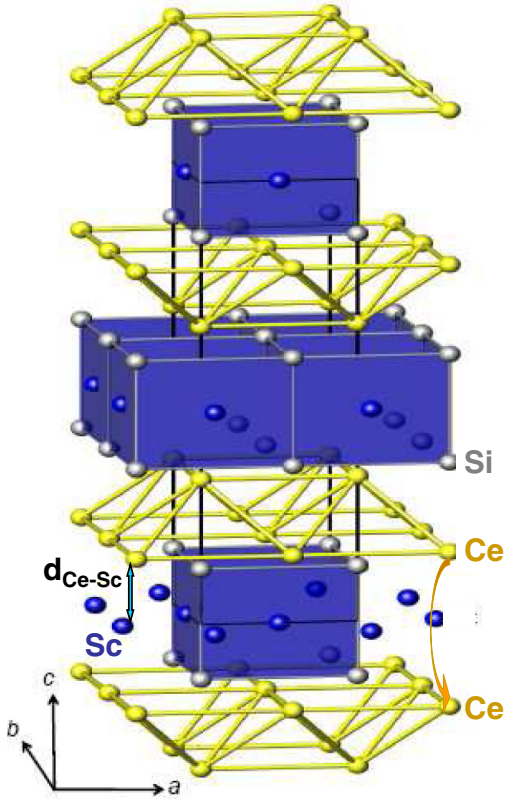

FIG. 1. (Color online) CeScSi-type structure, showing double Ce layers (yellow open network) and ligands layers (blue full network). Left side: $d_{Ce\text{-}Sc}$ indicates Ce-Sc spacing. Right side: curved arrow represents Sc mediated Ce-interlayers interaction.

The variation of $\chi(T)$ around the magnetic transition is shown in Fig. 4 (using a double logarithmic representation) for alloys with $x \geqslant 0.60$. The respective maxima of $\chi(T)$ between $20 \leqslant T_N \leqslant 50$ K indicate the AFM character of the magnetic transition. The samples with $x \leqslant 0.50$ are included

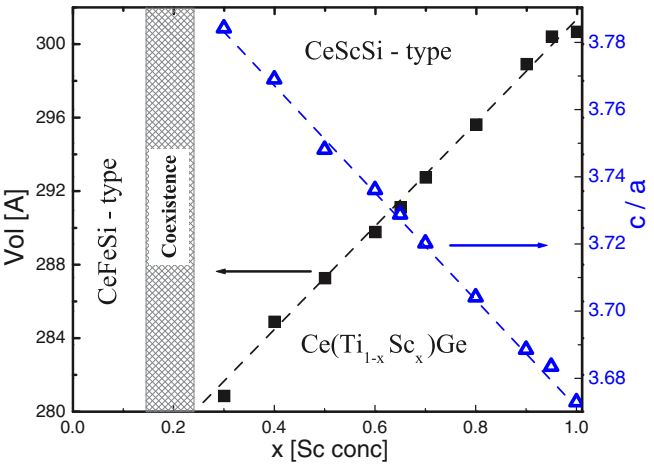

FIG. 2. (Color online) Unit cell volume variation in $CeTi_{1-x}Sc_xGe$ as a function of Sc content (left axis) and c/a lattice parameters ratio (right axis). Straight lines are guides to the eyes. The shaded area indicates the coexistence region of both structures.

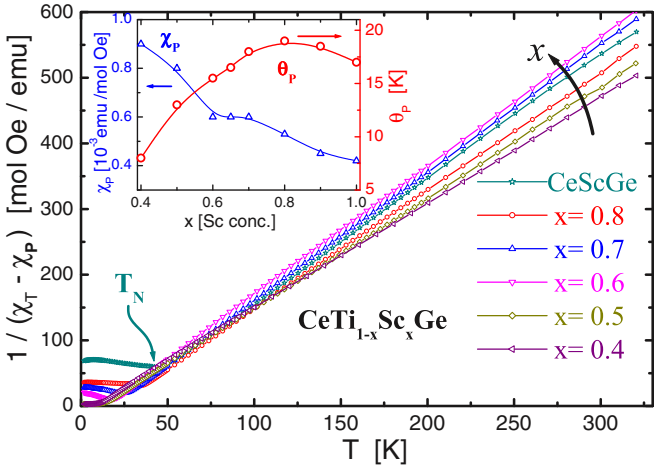

FIG. 3. (Color online) Inverse high temperature magnetic susceptibility measured in a field of $H = 10$ kOe, after subtracting a Pauli χ_P contribution. Inset: $\chi_P(x)$ contribution (left axis) and paramagnetic temperature $\theta_P(x)$ (right axis).

in the inset of Fig. 4 using a more extended $M(T)$ scale because of their FM character. The typical $M(T)$ dependence of a FM is observed for $x = 0.25$ and 0.3 alloys, whereas those with $x \geqslant 0.4$ show an incipient AFM component even in field cooling procedure. The thermal dependence in the paramagnetic phase is compared in the main figure with a general Curie-Weiss function $\chi(T) = 0.56/(T - 15.5)$ emu/Oe mol (notice the positive $\theta_P = 15.5$ K) to demonstrate the stability of the paramagnetic phase along the full concentration range. On the ordered phase, $\chi(T < T_N)$ shows a smooth behavior with the presence of a weak maximum at $T = T_L$ barely detected between $0.65 \leqslant x \leqslant 0.80$. This anomaly is better observed in specific heat measurements and its origin is discussed in the context of the magnetic phase diagram.

Those different behaviors can be sorted into three ranges of Sc concentration: (i) for $x \leqslant 0.6$ the $M(T)$ dependence

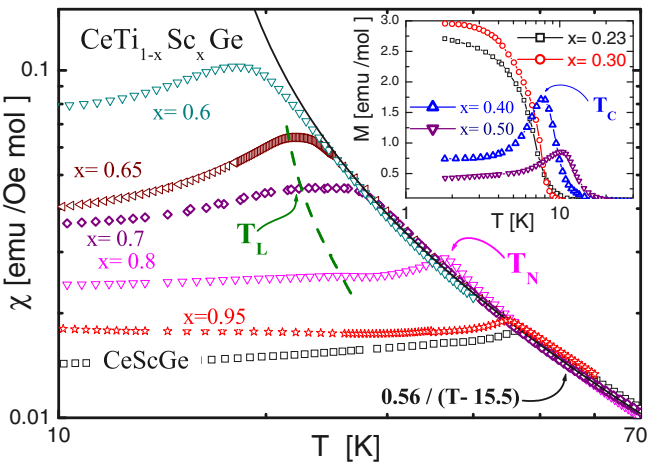

FIG. 4. (Color online) Low field ($H = 100$ Oe) magnetic susceptibility in a double logarithmic representation. Full curve is a reference for the paramagnetic phase (see the text) and dashed curve indicates the position of the second transition at $T = T_L$. Inset $M(T)$ measurements for $x \leqslant 0.50$ samples.

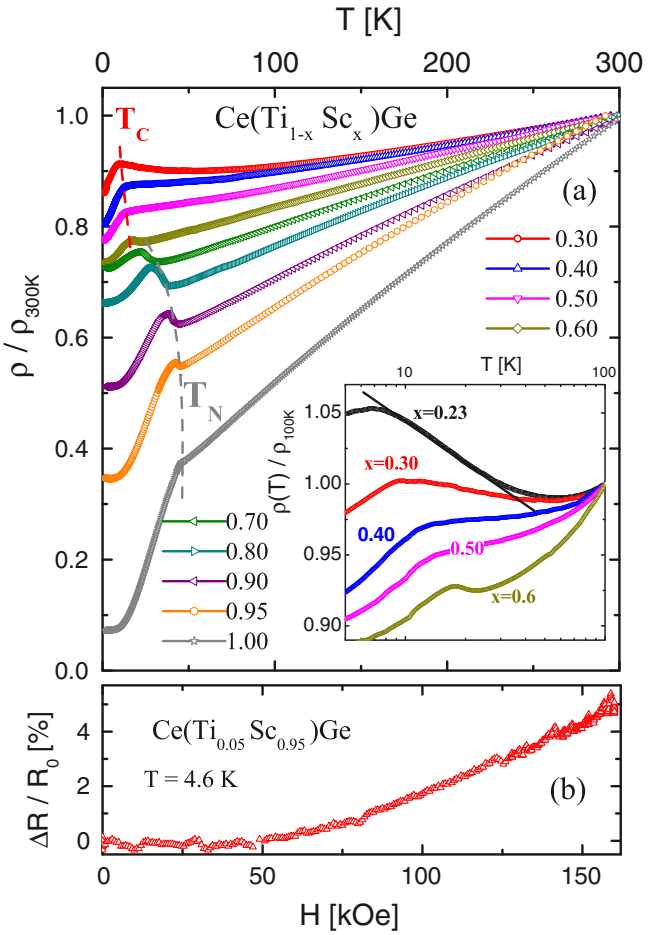

FIG. 5. (Color online) (a) Electrical resistivity normalized at 300 K of all measured samples. Inset: detail of the logarithmic T dependence of samples between $0.23 \leqslant x \leqslant 0.4$ normalized at 100 K for better comparison. (b) Percent magnetoresistance increase up to $H = 160$ K Oe.

indicates an increasing mixture of an AFM component in the dominant FM in the GS, with the ordering temperature increasing from $T_{ord} = 7$ K at $x = 0.25$ up to 16 K at $x = 0.60$. At $x = 0.65$ the $\chi(T)$ maximum displays two shoulders which can be distinguished after a detailed analysis of the $\chi(T)$ curvature, i.e., its second derivative $\partial^2\chi/\partial T^2$. This feature reveals that the $x = 0.65$ concentration is placed very close to a critical point. (ii) Between $0.65 \leqslant x \leqslant 0.8$, a slight kink appears at $T = T_L(x)$, below T_N, as seen in Fig. 4. Within this range of concentration, T_N increases from 19 K at $x = 0.65$ up to 35 K at $x = 0.8$, whereas $T_L(x)$ increases from 18 K up to 26 K. (iii) Above $x = 0.9$, T_N keeps growing from 38 K at $x = 0.9$ up to 47 K at $x = 1$, whereas $T_L(x)$ is hardly seen in $\chi(T)$ measurements.

C. Electrical resistivity

The thermal dependence of the electrical resistivity ρ, normalized at 300 K, is presented in Fig. 5(a) for samples between $0.30 \leqslant x \leqslant 1.0$. The rough ρ values at 300 K show a dispersion of about 20% around a mean value of 220 $\mu\Omega$ cm, with a tendency to a maximum at $x = 0.8$. That dispersion

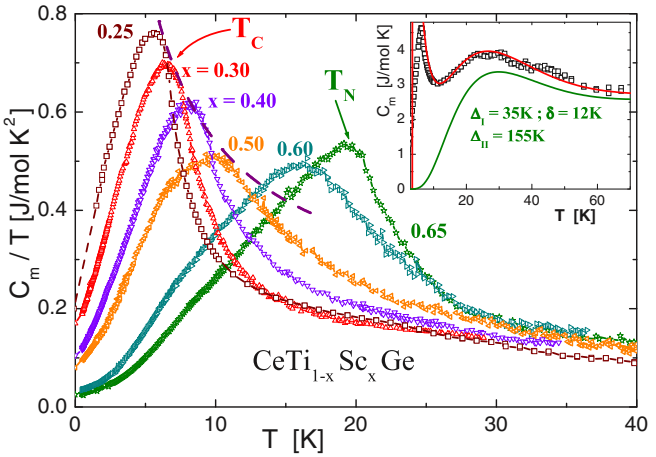

FIG. 6. (Color online) Magnetic contribution to the specific heat divided temperature within the $0.25 \leqslant x \leqslant 0.65$ range. Doted curve indicates the $1/T_{\rm ord}$ decreasing trend of the maximum below $x = 0.5$. Inset: fit of $C_m(T)$ for sample $x = 0.25$ at high temperature to evaluate the CEF spectrum; see the text.

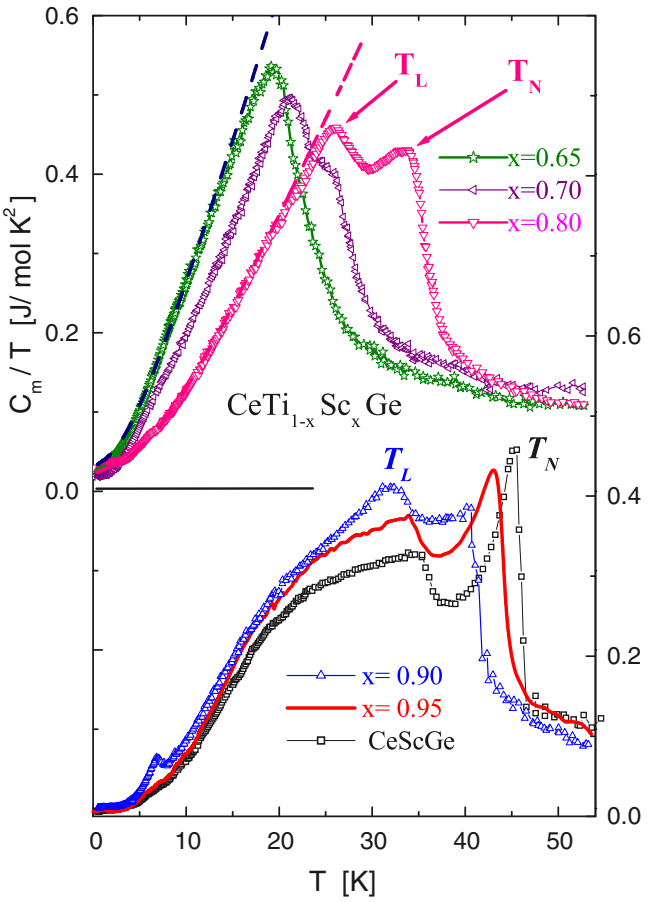

FIG. 7. (Color online) Magnetic contribution to the specific heat in the $0.65 \leqslant x \leqslant 0.80$ range (left axis), and the $0.90 \leqslant x \leqslant 1$ samples shifted for clarity (right axis). Dashed curves represent the fits on the ordered phase of samples $x = 0.65$ and 0.80 (see the text).

is attributed to random microcracks in the samples. The continuous increase of the $\rho(T)$ slopes indicates the weakening of Kondo type scattering with growing Sc content. In the inset of that figure, a detail of the logarithmic dependence of samples on the Ti-rich side ($0.23 \leqslant x \leqslant 0.60$) normalized at 100 K are collected to better analyze the role of the Kondo effect. A logarithmic increase of $\rho(T)$ approaching the magnetic transition from high temperature is observed at $x = 0.23$ as an indication of Kondo scattering contribution. However, the intensity of this electronic scattering rapidly decreases with Sc concentration until it vanishes at $x = 0.60$. At that concentration, a resistivity upturn characteristic of the opening of a gap in the Fermi surface emerges. This anomaly develops up $x = 0.80$ and then decreases again as the system reaches its stoichiometric CeScGe limit.

The change of the $\rho(T)$ dependence at $T = T_{\rm ord}$ is in agreement with the transitions observed from magnetic measurements. In the FM region a downward kink in $\rho(T)$ is observed at $T_{\rm ord}$, whereas a gap opening, usually related to AFM order, occurs for $x > 0.50$. Beyond the critical concentration, the width of the anomaly exceeds the temperature difference between T_N and T_L. The weakening of the $\rho(T)$ anomaly approaching the stoichiometric limit can be attributed to the variation of the Fermi level within the energy gap associated to the AFM state. As Ti^{4+} atoms are replaced by Sc^{3+} ones, the chemical potential decreases and eventually approaches the lower energy side of the gap. This simple picture has to be considered within the complexity of the Fermi surface in a system with many conduction electrons.

D. Specific heat

Specific heat results show several peculiar features along the full concentration range in coincidence with the different regimes observed in magnetic measurements. The results obtained on the $0.25 \leqslant x \leqslant 0.65$ alloys are presented in Fig. 6 as C_m/T, where C_m indicates the magnetic contribution to the specific heat after phonon subtraction. Within the experimental accuracy, the maxima of $C_m(x)/T$ coincide with those observed in $M(T)$. A common feature along this concentration range is the lack of a C_m jump at $T = T_{\rm ord}$. Instead, a broadened transition is observed, followed by a tail in $C_m/T(T > T_{\rm ord})$ that reveals a significant contribution of magnetic correlations as precursors of the magnetic transition. This tail becomes more extended in temperature with increasing $T_{\rm ord}(x)$ up to $x = 0.50$. Samples with $x = 0.60$ and $x = 0.65$ recover a larger slope just above $T_{\rm ord}$ together with a moderate increase of the C_m/T maximum. This change of tendency coincides with the modification of the magnetic structure around $x = 0.50$. In this concentration range, the maximum of C_m/T decreases as $\propto 1/T_{\rm ord}$. Although such a decrease is a consequence of plotting $C_m(T)/T$, it reveals that $C_m(T_{\rm ord})$ remains almost constant with decreasing $T_{\rm ord}$ and does not extrapolate to zero as one would expect in the case of a quantum critical point.

An increase of the low temperature curvature in $C_m(T)/T$ indicates a progressive opening of a gap of anisotropy (Γ) in the magnon spectrum with concentration. To evaluate that evolution, the low temperature C_m/T dependence was analyzed using the function $C_m/T = \gamma_0 + B \times T \times \exp(-\Gamma/T)$ as shown in Fig. 7 for samples with $x = 0.65$ and 0.8. The values

computed for those concentrations are $\Gamma(x = 0.65) = 7$ K and $\Gamma(x = 0.80) = 15$ K, respectively. Concerning the $\gamma_0(x)$ dependence, it drops from $\gamma_0 \approx 220$ mJ mol^{-1}K^{-2} at $x = 0.25$ down to $\approx$20 mJ mol^{-1}K^{-2} at $x = 0.60$.

The main characteristic of the alloys with $x > 0.65$ is the split of C_m/T into two maxima, in agreement with the $\chi(T)$ results. While the lower transition (at $T = T_L$) shows a cusplike anomaly between $x = 0.7$ and 0.9, the upper one (T_N) is associated to a jump in $C_m/T(T_N)$. Such a split cannot be distinguished in $C_m(T)$ nor in $M(T)$ measurements on the $x = 0.65$ sample. However, in preliminary thermopower measurements a maximum and a marked shoulder are observed at 21 and 23 K, respectively.

For $x \geqslant 0.9$, a further change in $C_m/T(T)$ is observed as depicted in the lower part of Fig. 7. The broad shoulder of $C_m/T(T)$ in samples $0.9 \leqslant x \leqslant 1$ can be attributed to the increase of the GS degeneracy from $N_{\rm eff} = 2$ to 4 as the contribution of the first exited CEF doublet gradually increases. Also both transitions change their aspects because, while the one at T_L transforms into a steplike anomaly, that at T_N becomes sharper and grows significantly. Notice that the $\Delta C_m(T_N)$ jump in $x = 1$ is $\approx$16 J mol^{-1}K^{-1}, in between the values predicted in a mean field approximation for a doublet ($\Delta C_m = 1.5R = 12.5$ J mol^{-1}K^{-1}) and a quartet ($\Delta C_m = 2.2R \approx 18$ J mol^{-1}K^{-1}) [18]. The small peak observed in $x = 0.9$ at $T \approx 7$ K can be attributed to an extrinsic contribution of a small amount of Ce oxide.

E. Magnetization

The $M(H)$ hysteresis loops measured at $T = 1.8$ K on the alloys with $x \leqslant 0.5$ reveal the FM character of the ordered phase [see Fig. 8(a)]. Measurements performed up to $H = 50$ K Oe are presented in Fig. 8(b) showing that at high magnetic field $M(x)$ increases up to a maximum value for $x = 0.50$. The saturation magnetization ($M_{\rm sat}$), extracted from Fig. 8(b) as $M(x,H) = M_{\rm sat} \times (1 - a/H)$, increases from $1.04\mu_B$/f.u. for $x = 0.30$ up to $1.15\mu_B$/f.u. for $x = 0.50$. At $x = 0.6$ $M_{\rm sat}$ decreases to $1\mu_B$/f.u., though this value is extracted from a reduced fitting range. Similarly, the coercive field increases from 1.1 K Oe for $x = 0.30$ up to 2.6 kOe for $x = 0.50$.

At $x = 0.60$, the spontaneous FM magnetization is replaced by a small susceptibility, indicating a transition to an AFM state. Coincidentally, a metamagnetic transition (MMT) appears with the critical field $H_{\rm cr}$ increasing with Sc concentration up to our experimental limit of $H = 50$ kOe with an initial ratio of $\partial H_{\rm cr}/\partial x = 2.2$ K Oe/Sc%.

In contrast with $M(H)$ measurements performed on stoichiometric CeScGe [15,17], which report a MMT transition around $H_{\rm cr} \approx 60$ K Oe with a weak associated hysteresis, no signal of MMT was observed in preliminary magnetoresistance measurements up to $H = 160$ K Oe on the Sc rich side. In Fig. 5(b) we show the monotonous increase of the positive magnetoresistence of $CeT_{0.05}Sc_{0.95}Ge$ in percent units $\Delta R/R_0$, where $\Delta R = R(H) - R_0$ with $R_0 = R(H = 0)$. Similar behavior is observed for CeScGe, both measured at $T = 4.6$ K. This disappearance of the MMT at high Sc concentration coincides with the decrease of the area of hysteresis loop in $M(H)$ as $H_{\rm cr}(x)$ increases, shown in Fig. 8(b).

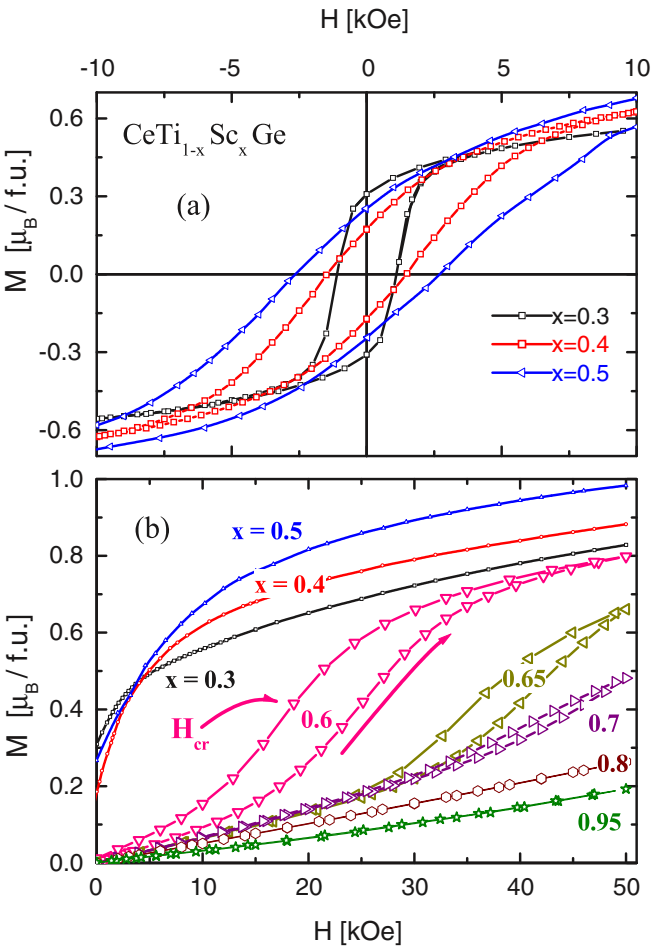

FIG. 8. (Color online) Magnetization measurements at $T = 1.8$ K: (a) hysteresis loops centered at $H = 0$ for the FM $0.3 \leqslant x \leqslant 0.5$ alloys. (b) Magnetization curves up to $H = 50$ kOe, showing a metamagnetic transformation in samples with $x \geqslant 0.6$.

III. DISCUSSION

A. Evaluation of the crystal electrical field splitting

In order to have a qualitative evaluation of the energy of the excited CEF levels we have analyzed the $C_m(T)$ dependence of the $x = 0.25$ sample which shows the lowest ordering temperature. For that purpose we have fitted the experimental data taking into account that the CEF splits the sixfold Hund's rule multiplet, originated in the $J = 5/2$ angular momentum of Ce, into three Kramer's doublets. Due to the eventual hybridization (i.e., Kondo effect) acting on the first excited level, the standard Schottky anomaly ($C_{\rm Sch}$) may not describe the $C_m(T)$ dependence properly. Thus a standard approach to mimic a broadening of the levels was applied. For this procedure the first CEF exited doublet at Δ_1 is described as a set of four single levels equally distributed in energy around the nominal value of the represented broadened level. This method is only applicable to weakly hybridized level (i.e., $\Delta_1/k_B > T_K$). To properly account for the total magnetic contribution to the entropy, a second excited doublet (at Δ_2) was included in the evaluation of the full CEF spectrum. Since Δ_2 largely exceeds the temperature range of our $C_m(T)$ measurements, no hybridization effects were taken into account for this analysis.

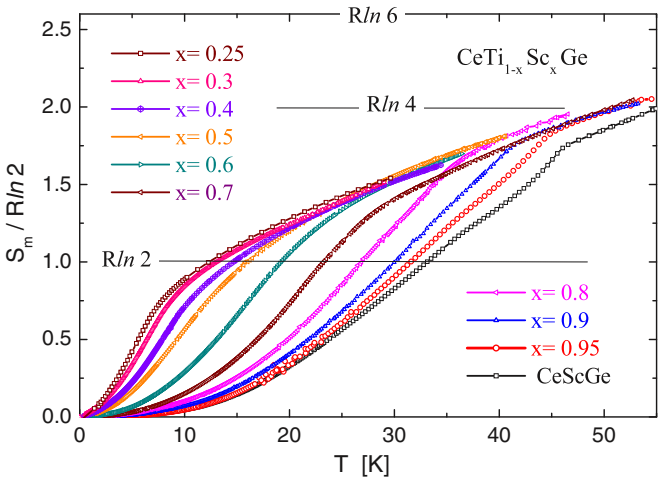

FIG. 9. (Color online) Thermal evolution of the magnetic contribution to the entropy (S_m) normalized by R ln 2.

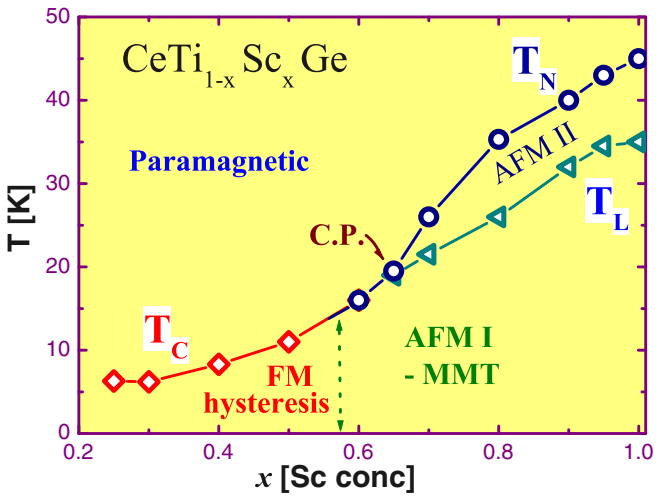

FIG. 10. (Color online) Sc concentration dependence of the magnetic phase diagram showing the transition temperatures extracted from magnetic and thermal measurements (left axis) within the range of the CeScSi-type structure.

The applied formula is

$$C_{\mathrm{Sch}}(T) = \Sigma_i A_i \left[\left(\frac{\Delta_i}{T} \right) \Big/ \cosh \left(\frac{\Delta_i}{T} \right) \right]^2 . \qquad (1)$$

Since the measured specific heat $C_m(T)$ contains GS (C_{GS}) and C_{Sch} contributions, the proper fit has to be performed adding both components: $C_m = C_{\mathrm{GS}}(T) + C_{\mathrm{Sch}}(T)$. In this case, C_{GS} corresponds to the high temperature tail of the magnetic anomaly of the $x = 0.25$ sample which can be properly described as $C_{\mathrm{GS}} \propto 1/T^2$. In the inset of Fig. 6 the result of this fit to the experimental data is shown, including the detail of the C_{Sch} function. The computed parameters are $\Delta_1 \approx 35$ K and $\Delta_2 \approx 155$ K, with an effective broadening of the first CEF doublet evaluated as $\delta = 12$ K. These results were checked with the evaluation of the magnetic entropy involved in this Schottky anomaly. This analysis cannot be applied for higher Sc concentrations because the increase of T_{ord} progressively approaches Δ_1. The analysis of the entropy collected at ≈50 K, see Fig. 9, excludes significant changes expected in the CEF levels splitting. Nevertheless, the reduction of the electrical charges at the transition metal sites from Ti^{4+} [Ar4$s^2$3d^2] to Sc^{3+} [Ar4$s^2$3d^1] may affect the CEF levels eigenfunctions with the consequent effect on the anisotropy and the magnetic interaction between neighboring planes.

B. Entropy

The analysis of the thermal evolution of the magnetic contribution to the entropy $S_m(T)$ is shown in Fig. 9 normalized by the value of a Kramer's doublet level: R ln 2. The alloy $x = 0.25$ with the lowest ordering temperature ($T_C = 7$ K) reaches $S_m = R$ ln 2 at $T = 11$ K, slightly above T_C, suggesting that only the GS doublet contributes to the magnetic order. However, since in the paramagnetic phase $S_m(T)$ increases continuously (i.e., without showing any plateau around R ln 2) one may infer that the low energy tail of the first excited CEF level starts to contribute to the entropy at quite low temperature. This fact qualitatively confirms the CEF level spectrum extracted in the previous subsection from the fit of $C_m(T)$.

Although the contribution of the first excited doublet to the ordered state may be marginal in the alloys with low Sc content, it becomes significant for higher concentrations as $S_m(T_{\mathrm{ord}})$ increases with $T_{\mathrm{ord}}(x)$. This feature becomes evident for $x \geqslant 0.5$ alloys because $S_m(T_{\mathrm{ord}})$ clearly exceeds R ln 2. Notice that around this concentration the AFM sets on. For $x = 1$ it practically reaches the value corresponding to two doublets, i.e., R ln 4, in agreement with the broad shoulder observed in $C_m(T)/T$ and the value of $\Delta C_m(T_N)$ (see Fig. 7).

The comparison of the entropy distribution above and below T_{ord} [i.e., $S_m(T < T_C)$ and $S_m(T > T_C)$, respectively] provides a hint to figure out the effective dimensionality of a magnetic system. According to theoretical predictions [19], for two dimensional (2D) systems the entropy accumulated between $T = 0$ and $T = T_{\mathrm{ord}}$ is similar to that contained in the tail of $C_m(T > T_{\mathrm{ord}})$. In this case, the samples with $0.25 \leqslant x \leqslant 0.5$ show $S_m(T < T_C)$ and $S_m(T > T_C)$ values close to the prediction for a simple square Ising lattice of spins 1/2. Such is not the case for samples beyond the critical concentration (i.e., $x \geqslant 0.65$) for which the shape of AFM transition tends to the characteristic $\Delta C_m(T_N)$ jump of a 3D second order transition. Also this change occurs around the modification of the magnetic character from FM to AFM.

C. Magnetic phase diagram

The magnetic characteristics of this system are summarized in the phase diagram presented in Fig. 10. The two most relevant features are the FM to AFM change between $0.50 \leqslant x \leqslant 0.60$. A critical point (CP) occurs at $x \approx 0.65$ where three phases, paramagnetic, AFM I, and AFM II, converge according to the phase boundaries defined by respective anomalies observed in the specific heat. There, an intermediate phase AFM II sets in between $T_N(x)$ and $T_L(x)$. Along the full concentration range different regions were identified as follows. (i) Between $0.25 \leqslant x \leqslant 0.50$ a FM-GS, as determined by M

vs H hysteresis loops of Fig. 6(a), shows an increasing M_{sat} that reaches its maximum value at $x = 0.50$. (ii) A continuous change from FM to AFM occurs between $0.50 < x < 0.60$, evidenced by the MMT with H_{cr} arising from zero. $\rho(T)$ measurements confirm this continuous change because the kink at $T = T_C$ progressively develops a characteristic AFM upturn (see Fig. 5) due to the opening of a gap in a fraction of the Fermi surface. (iii) Around the CP ($x \approx 0.65$) a weak transition emerges at $T_L(x)$ below T_N according to $C_m(T)$ and $\chi(T)$ results. Notably, $T_N(x)$ rises continuously up to $T_N = 47$ K (at $x = 1$) despite the weakening of the Ce effective magnetic moment.

As it was mentioned in the Introduction, there are early band-structure calculations [14] based on an itinerant character of CeScGe, that requires one to have at least a moderate hybridization between Ce-4f conduction states. Such exchange is typically manifested as an increase of $\rho(T)$ at low temperature, due to Kondo scattering, and the density of states reflected in γ_0. None of these effects are observed on the Sc-rich limit. On the contrary, they appear on the Ti-rich side despite the FM behavior. Since $\rho(T,x)$ and $\gamma_0(x)$ indicate a weakening of this interaction with Sc content, the high T_N value observed in CeScGe cannot be attributed to any hybridization mechanism but rather to an intrinsically strong Ruderman-Kittel-Kasuya-Yosida (RKKY) interaction.

A general description of the magnetic evolution of this system can be proposed by considering each Ce-double layer as a nearly 2D-FM unit that weakly interacts with neighboring layers. The positive and even growing $\theta_P(x)$ values support an increasing *intra*layer Ce-Ce neighbors FM interaction. Once the amount of Sc-3d^1 electrons becomes relevant (at $x \approx 0.50$) the *inter*layers RKKY interaction takes over favoring an AFM stacking of the double layers within an anisotropic but 3D scenario. The thermal population of the first CEF excited level also contributes to the FM-AFM change because of the modification of the involved moments.

Despite the ≈12% difference between Ti and Sc Goldschmit metallic radii ($r_{Ti} = 1.46$ Å and $r_{Sc} = 1.64$ Å, respectively), the Ce-T spacing ($d_{Ce\text{-}T}$) only increases by ≈2% between CeTiGe ($d_{Ce\text{-}Ti} = 3.45$ Å [20]) and CeScGe ($d_{Ce\text{-}Sc} = 3.53$ Å [15]) evaluated within the same CeScSi structure. This variation is in agreement with the slight change (≈1%) observed on the c axis between $x = 0.30$ and $x = 1$. Within a *rigid sphere* picture, this $d_{Ce\text{-}Sc} = 3.53$ Å and the sum of Sc and Ce metallic radii ($r_{Sc} = 1.64$ Å and $r_{Ce} = 1.86$ Å) become comparable. Therefore, a significant increase of the electronic overlap between Sc-3d and Ce-5d electrons can be expected with the consequent strengthening of the Ce-*inter*layers RKKY interaction.

In this context one should notice that isotypic rare earth (R) compounds of the RTGe family also present very high ordering temperatures, like GdScGe (CeScSi type structure) that orders at $T_C = 350$ K [21], more than a factor 7 higher than in CeScGe. Similar values are observed for GdTiGe (of CeFeSi type structure) with $T_N = 412$ K [22]. These behaviors are in clear contrast with itinerant cases like $CeRh_2Si_2$ and $CeRh_3B_2$ [2,7], for which the T_N ratio between $GdRh_2Si_2$ and $CeRh_2Si_2$ is only a factor 3.

IV. CONCLUSIONS

Apart from the significantly high ordering temperature of CeScGe at $T_N = 47$ K, the main magnetic characteristics shown by this system are the continuous change from FM to AFM-I order and the presence of a CP point (at $x = 0.65$) associated to an intermediate AFM-II phase. These modifications of the magnetic ground state occur without affecting the local character of the Ce-4f orbital.

The layer type of the crystalline structure seems to play a basic role because it favors the formation of FM sheets involving two neighboring Ce planes. At low Sc content ($0.25 \leqslant x \leqslant 0.50$) the FM *intra*plane RKKY interaction, resembling 2D-type order, dominates the scenario. The continuous increase of the positive θ_P temperature indicates that this Ce-Ce interaction even enhances with concentration.

After reaching the maximum of M_{sat} at $x = 0.50$, the system develops a MMT transition from $H_{cr} = 0$. Such a continuous transition from a FM state to an AFM reveals the similar energy of these competing phases, that can be described as a smooth modification from a FM stacking to an AFM stacking of FM layers. This change in the *inter*layers RKKY interaction can be driven by the variation of the electronic configuration of the intermediaries atoms Ti^{4+} and Sc^{3+}.

The increasing *inter*layers interaction strengthens the 3D character of the AFM phase evidenced by the $C_m(T)$ jump at the magnetic transition. The appearance of an intermediate phase AFM-II indicates that the magnetic order parameter changes before reaching the ground state configuration. The $S_m(T,x)$ evolution confirms the first excited CEF level increasing contribution as T_N becomes comparable to Δ_1. Therefore, the record high ordering temperature of CeScGe has to be attributed to the convergence of different factors, such as the Ce double-layer structure of FM character, the increasing RKKY interaction with Sc-3d^1 concentration, and the vicinity of the first CEF excited level. All these conditions are related with the local characters of the Ce-4f orbitals.

ACKNOWLEDGMENTS

This work was partially supported by ANPCyT (Grant No. 2010-1060) and SECyT-UNCuyo (Grant No. 06/C457). J.G.S., P.P., and M.G.B. acknowledge support as members of CONICET, while S.E. acknowledges support in the form of a scholarship.

[1] R. A. Fisher, E. W. Hornung, G. E. Brodale, and W. F. Giauque, J. Chem. Phys. **58**, 5584 (1973).

[2] S. K. Malik, R. Vijayaraghavan, and W. E. Wallace, J. Magn. Magn. Mater. **37**, 303 (1983).

[3] See, for example, E. Bauer, Adv. Phys. **40**, 417 (1991).

[4] See, for example, J. G. Sereni, in *Handbook Phys Chem of Rare Earths*, edited by K. A. Gschneidner, Jr. and L. Eyring (Elsevier Science Publishers, B. V., 1991), Vol. 15, Chap. 98; J. Phys. Soc. Jpn. **67**, 1767 (1998) and references therein.

[5] L. E. De Long, J. F. Huber, and K. S. Bedell, J. Magn. Magn. Mater. **99**, 171 (1991).
[6] P. C. Canfield, J. D. Thompson, and Z. Fisk, J. Appl. Phys. **70**, 5992 (1991).
[7] C. Godard, L. C. Gupta, and M. F. Ravet-Krill, J. Less-Common Met. **94**, 187 (1983).
[8] See, for example, S. Kawarazaki, M. Sato, Y. Miyako, N. Chigusa, K. Watanabe, N. Metoki, Y. Koike, and M. Nishi, Phys. Rev. B **61**, 4167 (2000).
[9] S. Kawarazaki, Y. Kobashi, J. A. Fernandez-Baca, S. Murayama, Y. Önuki, and Y. Miyako, Physica B **206-207**, 298 (1995).
[10] R. Settai, A. Misawa, S. Araki, M. Koski, K. Sigiyama, T. Takeuchi, K. Kindo, Y. Haga, E. Yamamamoto, and Y. Önuki, J. Phys. Soc. Jpn. **66**, 2260 (1997).
[11] M. Gómez Berisso, P. Pedrazzini, J. G. Sereni, O. Trovarelli, C. Geibel, and F. Steglich, Eur. Phys. J. B **30**, 343 (2002).
[12] A. R. Mackintosh, Physica B **130**, 112 (1985).
[13] S. Doniach, Physica B **91**, 231 (1977).
[14] T. Shigeoka, M. Yokohama, M. Kosaka, Y. Uwatoko, M. Furugen, S. Ishida, and S. Asano, Physica B **281-282**, 96 (2000).
[15] S. Singh, S. K. Dhar, C. Mitra, P. Paulose, P. Mainfrinetti, and A. Palenzona, J. Phys.: Condens. Matter **13**, 3753 (2001).
[16] T. Gruner, N. Caroca-Canales, O. Stocker, M. M. Koza, J. Sereni, U. Burkhard, and C. Geibel (unpublished).
[17] Y. Uwatoko, T. Ishii, G. Oomi, H. Takahashi, N. Môri, S. Nimori, G. Kido, J. L. Serrao, D. Mandrus, Z. Fisk, and J. D. Thompson, Physica B **237-238**, 207 (1997).
[18] See, for example, P. H. Meijer, J. H. Colwell, and B. P. Shah, Am. J. Phys. **41**, 332 (1973).
[19] See, for example, C. Domb and A. R. Miedema, in *Progress in Low Temperature Physics*, edited by C. J. Gorter (North Holland, 1964), Vol. IV, Chap. VI, p. 300.
[20] B. Chevalier, W. Hermes, E. Gaudin, and R. Pottgen, J. Phys.: Condens. Matter **22**, 146003 (2010).
[21] S. Couillaud, E. Gaudin, V. Franco, A. Conde, R. Pöttgen, B. Heying, U. Ch. Rodewald, B. Chevalier *et al.*, Intermetallics **19**, 1573 (2011).
[22] S. A. Nikitin, I. A. Tskhadadze, I. V. Telegina, A. V. Morozkin, and Y. Seropegin, J. Magn. Magn. Mater. **182**, 375 (1998).